

INVESTIGATION OF INTERBAND TRANSITIONS IN FERROMAGNETIC METALS AND ALLOYS BY THE MAGNETO-OPTICAL METHOD

G. S. KRINCHIK and V. S. GUSHCHIN

Moscow State University

Submitted April 16, 1969

Zh. Eksp. Teor. Fiz. 56, 1833—1842 (June, 1969)

The results are reported of the first low-temperature magneto-optical measurements carried out on Ni, Fe, Co and some binary alloys in the 0.23—5.4 eV range. The anomalies observed in the equatorial Kerr effect in Ni are attributed to the edges of interband optical transitions in the vicinity of the L, W, and X symmetry points of the Brillouin zone, which can be used to determine the band parameters and the exchange splitting of the d and p bands. Co exhibits a strong anomaly at 0.7—1.0 eV which has a fine structure at low temperatures. Qualitative conclusions are drawn about changes in the nature of the electron states in these metals due to a shift away from the Fermi level or due to variation of the temperature, the impurity concentration, and the number of holes in the 3d band.

ONE of the more important current concerns in solid-state physics is the electron structure of metals belonging to the transition groups. Magneto-optical methods can be useful in studies of this particular area for two reasons. First, the singularities (critical frequencies) in the dependences of the magneto-optical effects on the energy of light quanta, observed in the short-wavelength region and attributed to definite interband transitions, can give quantitative information on the band structure of a metal, the exchange and spin-orbit splitting, the nature of electron states located far from the Fermi level, etc. Secondly, measurements of the magneto-optical effects in the long-wavelength region provide an effective method for investigating the high-frequency conductivity of a ferromagnetic metal, the nature of carrier scattering, the many-electron effects in the metal, the behavior of the ferromagnetic Hall effect at optical frequencies, etc. The present paper deals with the first of these two aspects. We investigated the frequency dependence of the equatorial Kerr effect of Ni, Co, Fe and of Ni—Cu, Ni—Mo alloys in a wide range of frequencies in the infrared, visible, and ultraviolet range in order to detect and identify the critical frequencies of the interband transitions. The magneto-optical measurements were carried out not only at room temperature but also at liquid nitrogen and helium temperatures in order to identify more easily the edges of interband transitions.

EXPERIMENTAL METHOD

A metal optical cryostat was used to carry out the magneto-optical measurements at low temperatures. A heat conductor, joining a sample with a helium bath, was made of crystalline quartz in which the axis of highest thermal conductivity coincided with the helium-sample direction. The central part of the cryostat was surrounded by an external glass screen, rectangular and measuring 15 × 40 mm. The shape of the glass screen and the positions of windows, shown in Fig. 1, made it possible to carry out measurements using large angles of incidence of light and to minimize the gap in the electromagnet which magnetized the sample at right-angles to the plane of incidence of the light. The metal parts

were replaced with glass and quartz in order to avoid heating by Foucault currents, as well as the vibrations of various parts of the cryostat under the influence of an alternating magnetizing field. For the same reason, the volume enclosed by a radiation screen was made as small as possible. This screen was fabricated from thin (0.2—0.25 mm) copper sheet. The gaps between the heat conductor, the radiation screen, and the external screen of the central part of the cryostat were 1.5—2 mm. Light entered the cryostat through fluorite windows. The temperature of the sample was 13° K when the cryostat was filled with liquid helium and 80° K when it was filled with liquid nitrogen.

We used the dynamic method for measuring the magneto-optical effects, described in^[1]. Figure 1 shows the basic layout of the apparatus used to measure the equatorial Kerr effect $\delta = \Delta I/I_0$, which was the relative change in the intensity of the reflected light when an alternating magnetic field was applied to the sample. The alternating magnetization of the sample was produced by a magnetic field of 2700 Oe generated by a small toroidal electromagnet (the gap between the poles was 17 mm), whose winding carried a current of 1.5 A. The electromagnet was supplied by a low-frequency power amplifier and a master oscillator at the amplifier input was tuned to a frequency of 78 Hz. The induc-

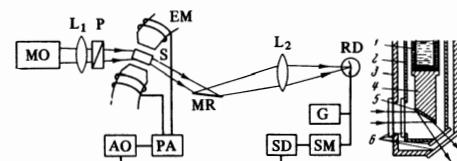


FIG. 1. Block diagram of the apparatus used to measure the equatorial Kerr effect: MO — monochromator; L₁, L₂ — lenses; P — polarizer; S — sample; MR — mirror; RD — radiation detector; EM — electromagnet; AO — audiofrequency oscillator; PA — power amplifier; G — mirror galvanometer; SM — selective microvoltmeter; SD — synchronous detector. The construction of the central part of the cryostat is shown on the right-hand side: 1) liquid helium bath; 2) radiation screen; 3) outer screen; 4) quartz heat conductor; 5) sample; 6) fluorite windows.

tance of the electromagnet winding was compensated by a suitable capacitor.

An IKM-1 infrared monochromator was used as the source of light in the 0.225–0.5 eV range, and a DMR-4 double monochromator was employed in the 0.5–5.4 eV range. The light flux was recorded, in the various ranges of wavelengths, by the following radiation detectors: an FEU-39A photomultiplier, a PbS photoresistor, and an InSb cooled photodiode. An electrical signal, proportional to the total intensity of the reflected light I_0 , was recorded by a mirror galvanometer and a modulated signal $\Delta I \sin \omega t$ was recorded by a V6-2 selective microvoltmeter and an SD-1 synchronous detector. The use of a synchronous detector in the measuring circuit and of low-noise radiation detectors made it possible to record effects of the order of 5×10^{-5} , i.e., it enabled us to increase the limit of reliable measurement of the signal by one order of magnitude.

The samples used in the measurements were in the form of plates, $0.2 \times 4.5 \times 11$ mm. A mirror-smooth surface was obtained by mechanical polishing. The samples were annealed in vacuum in order to relieve mechanical stresses. Before the measurements, the samples were polished electrolytically. The purity of the Fe, Co, and Ni samples was not less than 99.99%.

EXPERIMENTAL RESULTS

The frequency dependences of the equatorial Kerr effect $\delta(\omega)$ of Ni, Fe, and Co are given in Figs. 2–4. The measurements were carried out at two angles of incidence of light (φ_1 and φ_2) and at three temperatures: 13, 80, and 295°K. Two angles of incidence of light were used in order to identify more reliably the singularities in the $\delta(\omega)$ curves and to enable us to calculate the non-

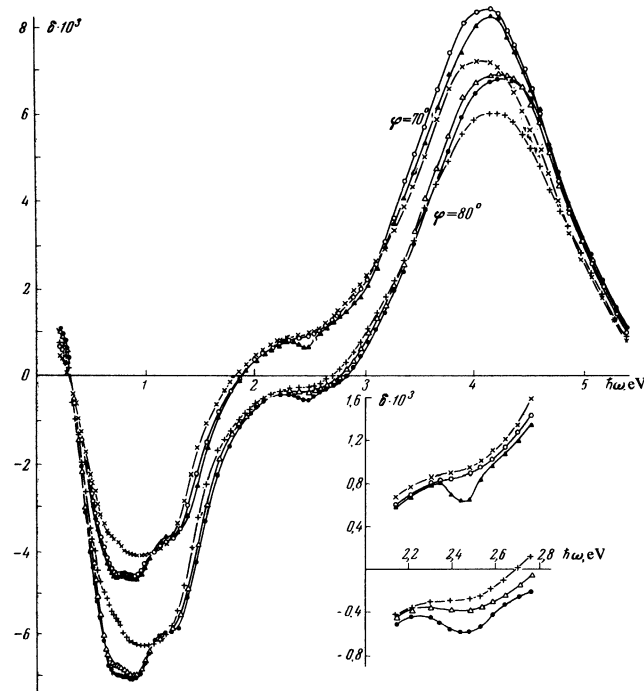


FIG. 2. Equatorial Kerr effect in Ni for two angles of incidence of light and for different temperatures (in °K). Case $\varphi = 70^\circ$: X) $T = 295$; O) $T = 80$; \blacktriangle) $T = 13$. Case $\varphi = 80^\circ$: +) $T = 295$; ∇) $T = 80$; \bullet) $T = 13$.

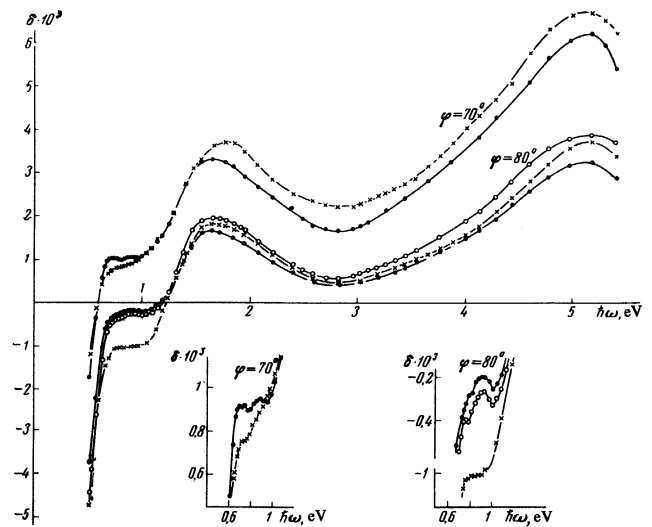


FIG. 3. Equatorial Kerr effect in Co for two angles of incidence of light at the following temperatures: X) 295, \bullet) 80, \circ) 13°K.

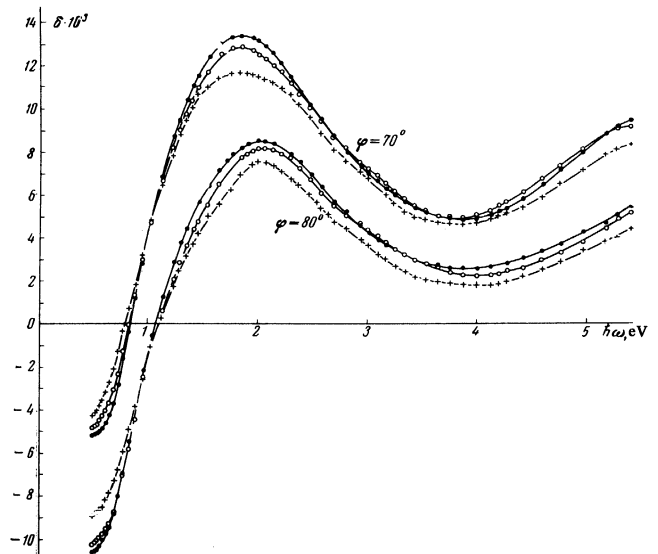


FIG. 4. Equatorial Kerr effect in Fe for two angles of incidence of light at the following temperatures: +) 295, \circ) 80, \bullet) 13°K.

diagonal components of the permittivity tensor $\epsilon_{xy} = -\epsilon_{yx} = i\epsilon'$, $\epsilon' = \epsilon'_1 - i\epsilon'_2$. A preliminary calculation, using optical constants taken from a table in [2] and from [3], showed that the dispersion curves $\epsilon'_1(\omega)$ and $\epsilon'_2(\omega)$ were in agreement with the results given in [3].

The $\delta(\omega)$ curves of Ni, obtained at $T = 80^\circ\text{K}$ and $T = 13^\circ\text{K}$, showed clearly singularities at 0.8, 1.3, and 2.5 eV; only the lowest-frequency singularity appeared at room temperature and therefore it was found previously by the magneto-optical method. [1] This singularity had a fine structure at low temperatures. Two kinks or weak maxima were located at 0.72 ± 0.02 and 0.9 ± 0.03 eV, i.e., the gap between the components was ~ 0.18 eV. Special measurements in the temperature range 80–300°K showed that the characteristic two-component nature of this anomaly appeared at 120°K. Figure 5 shows three of the equatorial Kerr effect curves, recorded in the energy range 0.5–1.5 eV, as well as the curve for a single crystal of Ni which

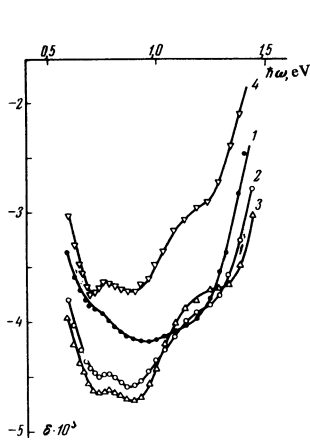


FIG. 5.

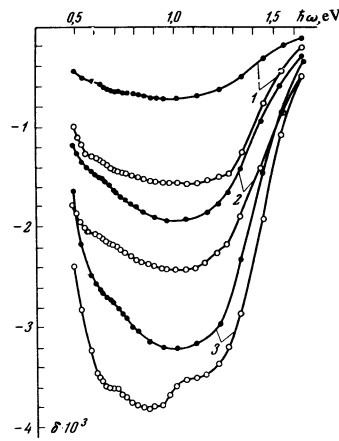


FIG. 6.

FIG. 5. Equatorial Kerr effect in Ni at the following temperatures: 1) 295, 2) 120, 3) 13°K. Curve 4 represents the results, obtained at 80°K, for a single crystal of Ni cut along the (110) plane. The values of δ are too low because of the large demagnetization factor for the angle $\varphi = 70^\circ$.

FIG. 6. Equatorial Kerr effect in the alloys: 1) 99% Ni-1% Mo, 2) 97% Ni-3% Mo, 3) 95% Ni-5% Mo (atomic percent) at two temperatures: ●) 295°K, ○) 13°K.

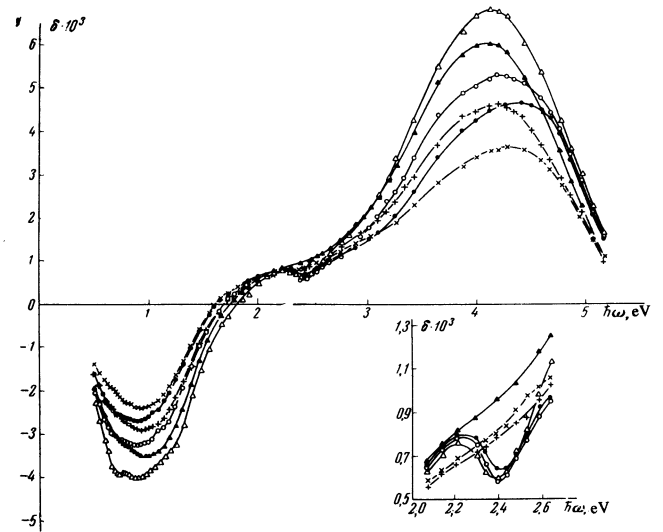


FIG. 7. Equatorial Kerr effect in the alloys: 95% Ni-5% Cu (Δ : T = 295°K; \triangle : T = 13°K), 90% Ni-10% Cu (+: T = 295°K; ○: T = 13°K), 85% Ni-15% Cu (x: T = 295°K; ●: T = 13°K; the compositions are given in atomic percent).

showed more clearly the fine structure of the singularity at 0.8 eV. The singularity in the region of 1.0–1.3 eV appeared during cooling. When the temperature was lowered, the right-hand edge of this singularity shifted to higher energies and exhibited its steepest slope at T = 13°K. The singularity near 2.5 eV appeared only at helium temperatures: it was practically invisible even at liquid nitrogen temperatures.

To determine the influence of an admixture on the position of the 0.8 eV anomaly, we carried out measurements on Ni-Mo alloys in the near infrared region where even a small amount of the admixture strongly reduced the saturation magnetization of the alloy. Figure 6 gives the frequency dependences of the Kerr effect, which show that alloying not only broadened this anomaly but also shifted it considerably in the direction of lower energies. Although the position of the anomaly was difficult to determine sufficiently accurately because of a reduction in the magnitude of the effect, we were able to estimate, for example, that the left edge of the anomaly of the alloy with 5 at. % Mo shifted to 0.56 eV, compared with 0.72 eV for pure Ni.

It is evident from Fig. 7 that the singularities characteristic of pure Ni were also observed in Ni-Cu alloys: the 2.5 eV anomaly was retained in the alloys and its nature was independent, within the limits of the experimental error, of the concentration of Cu; the anomaly in the region of 1.0–1.3 eV decreased in magnitude and the anomaly at 0.8 eV practically disappeared.

As reported in [3], Co had a singularity in the region of 0.7–1.0 eV. This anomaly became clearer at low temperatures (Fig. 3) and exhibited a fine structure which was clearly visible both at 80 and 13°K for the $\varphi = 80^\circ$ angle of incidence of light. The positions of the components of this anomaly could be described either as two maxima at 0.74 ± 0.02 and 0.9 ± 0.02 eV or as two minima at 0.79 ± 0.02 and 0.97 ± 0.02 eV.

DISCUSSION OF RESULTS

The structure of the 0.8 eV anomaly of Ni, observed at low temperatures (Figs. 2 and 5), has been interpreted by us as the result of the spin-orbit splitting of the interband transition edge $L_{1\uparrow} \rightarrow E_F$ (Fig. 8). This experimental observation was used in [4] to refine the electron structure of ferromagnetic Ni in the vicinity of the L point of the Brillouin zone. The reasoning is as follows.

Since transitions in the sub-band of the right-handed spins (the magnetic moments parallel to I_S) are possible only in the transverse direction $L \rightarrow W$, for which the spin-orbit components at 0.72 and 0.9 eV in the $\delta(\omega)$ curves should be attributed to the edges of interband transitions in the sub-band of the left-handed spins (\downarrow in Fig. 8). The \downarrow sub-band has two spin-orbit-split edges of the interband transitions $L_{2\downarrow}' \rightarrow L_{32}$ (transition

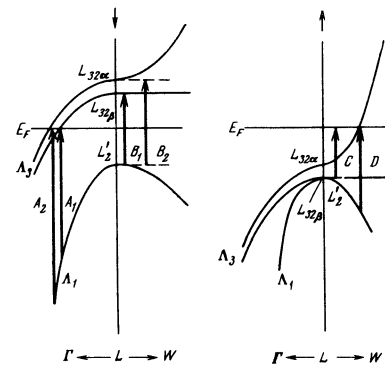


FIG. 8. Model of the band structure of ferromagnetic Ni near the L point of the Brillouin zone. The arrows at the top of the figure denote the sub-bands of the left-handed (\downarrow) and right-handed (\uparrow) spins. The subscripts α and β are used to denote the spin-orbit-split components of the L_{32} level.

B) and $\Lambda_{1\uparrow} \rightarrow E_F$ (transition A). The B transition should be rejected because a theoretical estimate of the width of the energy gap $\hbar\omega_{B_1} - \hbar\omega_{B_2}$ is considerably smaller than the experimental value of 0.18 eV. It follows from Fig. 8 that the difference $\hbar\omega_{B_2} - \hbar\omega_{B_1}$ should have the same order of magnitude as the spin-orbit splitting parameter of the 3d function of free Ni ions, i.e., it should not exceed 0.06 eV.^[5] On the other hand, the splitting of the A transition may be larger if the effective mass is given by the inequality $m_{\parallel}(L_{32\uparrow}) > m_{\parallel}(L'_{2\uparrow})$. Moreover, the attribution of the anomaly at 0.8 eV to the B transition shifts the zero point of ϵ'_2 (the imaginary part of the nondiagonal component of the permittivity tensor) into the region $\hbar\omega > 1.0$ eV, which does not agree with the experimental data.^[1,3]

We shall use our attribution of the spin-orbit components to the A_1 and A_2 transitions, as well as the published results of the measurements of the de Haas–van Alphen effect, magnetoresistance, and temperature-modulated reflectance, to consider the band parameters of ferromagnetic Ni using the model with the reverse order of levels^[6] (cf. Fig. 8). The effective mass $m_{\perp}(L_{32\alpha\uparrow})$ can be determined from the experimental value of the neck diameter of the Fermi surface of Ni on the assumption that the many-body effective mass enhancement factor is $\beta = 1.7$. This value of β is equal to the experimental value of β for Pt^[7] and, moreover, when this value of the factor is used, the gap $E_F - E(L_{32\alpha\uparrow}) = 0.19$ eV, as well as the edge of the interband C transition, can be identified with the long-wavelength resonance at 0.25 eV found in experiments on the temperature modulation of the reflectance carried out by Hanus et al.^[8] Hanus et al. also observed a similar temperature-modulated reflectance maximum at 0.4 eV, which could be attributed, in the model used, to the D transition. Bearing in mind that a theoretical estimate gives the ratio $m_{\perp}(L_{32\alpha\uparrow})/m_{\perp}(L'_{2\uparrow}) \approx 0.8$,^[9] we can find the effective mass $m_{\perp}(L'_{2\uparrow})$ and the energy gap $E_F - E(L'_{2\uparrow})$.

An assumption that a change of sign of ϵ'_2 is due to the activation of transitions in the sub-band of the left-handed spins in the region of 0.4 eV (transition B)^[6] makes it possible to identify the B_1 and B_2 transitions with two negative maxima of the temperature-modulated reflectance at 0.36 and 0.42 eV.^[8] The effective masses $m_{\parallel}(L_{32})$ are found from the condition $m_{\parallel}(L_{32\alpha\uparrow}) \approx m_{\parallel}(L_{32\beta\uparrow}) \approx m_{\parallel}(L_{32\beta\downarrow}) \approx m_{\parallel}(L_{32\alpha\downarrow})$, which is based on the observation that, in the longitudinal direction, the d band does not interact with the p band. Since the ratio $m_{\parallel}(L_{32\alpha\uparrow})/m_{\perp}(L_{32\alpha\uparrow}) = 2.5$ is known from the data on the de Haas–van Alphen effect,^[10] we can calculate $m_{\parallel}(L_{32\alpha\uparrow})$ from the value obtained for $m_{\perp}(L_{32\alpha\uparrow})$. Using $\hbar\omega_{B_1} = 0.36$ eV, $\hbar\omega_{A_1} = 0.72$ eV, $\hbar\omega_{A_2} = 0.9$ eV, we can find $m_{\parallel}(L'_{2\uparrow})$ and the energy gaps $E(L_{32\beta\uparrow}) - E_F$ and $E_F - E(L'_{2\uparrow})$.

The values of the transverse effective masses $m_{\perp}(L'_{2\uparrow})$ and $m_{\perp}(L_{32\alpha\uparrow})$ do not affect the positions of the interband transition edges and, therefore, we can estimate only their orders of magnitude by comparing the experimental and calculated data for the equatorial Kerr effect.^[4]

We shall now give the values¹⁾ of the band parameters of ferromagnetic nickel in the vicinity of the L point of the Brillouin zone, obtained as described in the present paper.

a) The sub-band of the left-handed spins:

$$\begin{aligned} E(L_{32\alpha\downarrow}) - E(L_{32\beta\downarrow}) &= 0,06(0,04), & E_F - E(L'_{2\downarrow}) &= 0,18(0,27), \\ E(L_{32\beta\downarrow}) - E_F &= 0,18(0,14), \\ \hbar\omega_{A_1} &= 0,72, & \hbar\omega_{A_2} &= 0,9(0,89), & \hbar\omega_{B_1} &= 0,36(0,38), & \hbar\omega_{B_2} &= 0,42, \\ m_{\parallel}(L'_{2\downarrow}) &= -0,13(0,09)m_0, & m_{\parallel}(L_{32\alpha\downarrow}) &= m_{\parallel}(L_{32\beta\downarrow}) = -0,4(0,37)m_0, \\ m_{\parallel}(L_{32\beta\downarrow})/m_{\parallel}(L'_{2\downarrow}) &= 3,0(4,2), \\ m_{\perp}(L_{32\beta\downarrow}) &= \infty & m_{\perp}(L'_{2\downarrow}) &= 3m_{\perp}(L'_{2\uparrow}), & m_{\perp}(L_{32\beta\downarrow}) &= 3m_{\perp}(L_{32\alpha\uparrow}); \end{aligned}$$

b) The sub-band of the right-handed spins:

$$\begin{aligned} E(L_{32\alpha\uparrow}) - E(L_{32\beta\uparrow}) &= 0,06(0,04), & E_F - E(L_{32\beta\uparrow}) &= 0,25(0,27), \\ E_F - E(L_{32\alpha\uparrow}) &= 0,19(0,21), \\ \hbar\omega_C &= 0,25, & \hbar\omega_D &= 0,4, \\ m_{\perp}(L_{32\alpha\uparrow}) &= 0,15(0,14)m_0, & m_{\perp}(L_{32\alpha\uparrow})/m_{\parallel}(L_{32\alpha\uparrow}) &= 0,38, \\ m_{\perp}(L_{32\alpha\uparrow})/m_{\perp}(L'_{2\uparrow}) &= 0,8, & m_{\perp}(L_{32\beta\uparrow}) &= \infty, \\ m_{\parallel}(L_{32\alpha\uparrow}) &= m_{\parallel}(L_{32\beta\uparrow}) = -0,4(0,37)m_0, & m_{\perp}(L'_{2\uparrow}) &= -0,19(0,18)m_0. \end{aligned}$$

It follows from these results that the exchange splitting of the d band is $\Delta E_d = E(L_{32\downarrow}) - E(L_{32\uparrow}) = 0.43(0.36)$ eV and the exchange splitting of the p band is $\Delta E_p = E(L'_{2\downarrow}) - E(L'_{2\uparrow}) = 0.07(0)$ eV. Some theoretical arguments in favor of ΔE_p being smaller than ΔE_d are given in^[9,12,13].

We must point out that the refinement of the values of the spin-orbit splitting parameters of the d band of Ni, the ratio $m_{\perp}(L_{32\alpha\uparrow})/m_{\perp}(L'_{2\uparrow})$, and the factor β gives rise to corresponding quantitative changes in the band structure parameters. These changes do not alter basically the band-structure model. However, since the absolute values of ΔE_p and $E(L_{32\uparrow}) - E(L'_{2\uparrow})$ are small, even slight changes in the parameters listed above may alter the sign of the exchange splitting of the p band ($\Delta E_p < 0$) or give rise to the normal order of levels in the sub-band of the right-handed spins [$E(L_{32\uparrow}) - E(L'_{2\uparrow}) < 0$]. Decisive data on this point would be provided by an experiment involving the determination of the sign of the p electron polarization in the vicinity of the L point in the Brillouin zone.^[14]

The high-energy singularities, observed by us at 1.3 and 2.5 eV, are obviously not associated with transitions in the vicinity of the L point of the Brillouin zone because transitions of the $L_{32} - L'_2$ type (analyzed by us) occur at lower energies and the energies of transitions of the $L_{31} \rightarrow L'_2$ type are far too high.^[13] The anomaly in the region of 1.3 eV may be attributed to the $W_{1\uparrow} \rightarrow W'_{1\uparrow}$ transition. The existence of a transition in this range of energies has been mentioned also in^[8,14,15]. The anomaly at 2.5 eV may be attributed to the $X_{5\uparrow} \rightarrow X'_{4\uparrow}$ transition, which is in agreement with the published band-structure calculations,^[13,16] according to which the energy of this transition is of the order of 2.8–3.0 eV.

¹⁾The energies are given in eV and m_0 denotes the electron mass. Values given in parentheses are obtained for a spin-orbit splitting parameter of 0.04 eV, which is about 35% larger than the atomic parameter and corresponds to the experimental value reported in [11].

It is evident from Fig. 7 that all the investigated anomalies are observed also in alloys with low concentrations of Cu but the low-energy anomalies at 0.8 and 1.3 eV broaden strongly when the concentration of Cu is increased and they practically disappear at 15 at. % Cu. However, the nature of the anomaly at 2.5 eV is not affected by an increase in the concentration of copper. We can see from Fig. 6 that when the temperature is increased the high-energy transitions broaden first (the anomaly at 0.8 eV can be seen even at room temperature although its structure can be observed only at low temperatures). On the other hand, an increase in the concentration of Cu in the alloys produces only a broadening of the low-energy transitions, leaving practically unaffected the 2.5 eV anomaly. Qualitatively, this can be explained as follows. The high-energy transitions correspond to electron states with shorter lifetimes and therefore the temperature must be lowered further to make the edges of interband transitions sufficiently steep. The addition of Cu to Ni produces a definite distortion of the potential and this distortion affects more strongly the broadening of the low-energy transitions. Finally, the "worst" broadening in the Fe, Co, Ni series is exhibited by the electron states of Fe, which—in contrast to Ni and Co—have a large number of holes in the $3d\uparrow$ sub-band.^[17] This possibly accounts for our failure to observe any clear singularities for Fe even at low transition frequencies and at liquid helium temperatures.

Cobalt exhibits a clear singularity in the low-energy range at 0.7–1.0 eV and this singularity has the characteristic low-temperature fine structure (cf. Fig. 3). The position and fine structure of this anomaly may be useful in the interpretation of the band structure of ferromagnetic Co. Unfortunately, in contrast to Ni, no detailed calculations of the energy bands of Co have yet been carried out and no thorough study of the band structure of the metal has yet been made using other experimental methods.

Finally, a shift of the 0.8 eV anomaly of Ni–Mo alloys in the direction of lower energies can be interpreted within the framework of the rigid band approximation using the proposed model of the electron structure of ferromagnetic Ni. The density of states in Ni, deduced from the specific heat,^[18] is 3.0 states per 1 eV · atom. The addition of 6 electrons per Mo atom, in the presence of 5 at. % Mo, gives rise—in the rigid band approximation—to an upward shift of the Fermi level by ~ 0.1 eV in the \uparrow sub-band and, consequently, yields the required shift of the position of the long-wavelength edge of the A_1 anomaly from 0.72 to 0.56 eV if the mass ratio is $m_{\parallel}(L_{32\uparrow})/m_{\parallel}(L'_{2\uparrow}) = 3$.

We must point out that the required shift of the positions of the anomalies of Ni–Mo alloys can be obtained ignoring the temperature dependence of the spontaneous magnetization and the corresponding change in the band structure in the ferromagnetic state. For example, although at room temperature the 0.8 eV anomaly of the 95% Ni–5% Mo alloy is strongly broadened, there is no reason to assume that it is shifted in the direction of long wavelengths compared with its position at $T = 80^\circ\text{K}$

although the saturation magnetization of the alloy increases approximately by a factor of 1.5 between 295 and 80°K . The cause of this effect is not yet clear but it may be associated with a transition from the ferromagnetic to the paramagnetic or antiferromagnetic ordering without an appreciable change in the Hund exchange splitting of the energy bands, suggested by Slater.^[12] A similar explanation of the gradual change of the Hall coefficient during passage through the Curie point has been given by Kondorskiĭ.^[19]

The authors are deeply grateful to Prof. A. J. de Vries and Dr. L. K. France, who kindly supplied us with a single crystal of pure Ni; to K. P. Myasnikova for the preparation of the samples of Ni–Mo alloys; and to I. S. Potapov and L. K. Vorob'ev for supplying the low-noise PbS detector.

¹G. S. Krinchik and G. M. Nurmukhamedov, *Zh. Eksp. Teor. Fiz.* 48, 34 (1965) [*Sov. Phys.-JETP* 21, 22 (1965)].

²H. H. Landolt and R. Börnstein, *Physikalisch-chemische Tabellen*, 8 vols., Springer Verlag, Berlin, 1923–1935.

³G. S. Krinchik and V. A. Artem'ev, *Zh. Eksp. Teor. Fiz.* 53, 1901 (1967) [*Sov. Phys.-JETP* 26, 1080 (1968)].

⁴G. S. Krinchik, V. S. Gushchin, and E. A. Gan'shina, *ZhETF Pis. Red.* 8, 53 (1968) [*JETP Lett.* 8, 31 (1968)].

⁵B. R. Cooper, *Phys. Rev.* 139, A1504 (1965).

⁶G. S. Krinchik and E. A. Ganshina, *Phys. Letters* 23, 294 (1966).

⁷J. B. Ketterson and L. R. Windmiller, *Phys. Rev. Letters* 20, 321 (1968).

⁸J. Hanus, J. Feinleib, and W. J. Scouler, *Phys. Rev. Letters* 19, 16 (1967); *J. Appl. Phys.* 39, 1272 (1968).

⁹J. C. Phillips, *J. Appl. Phys.* 39, 755 (1968).

¹⁰A. S. Joseph and A. C. Thorsen, *Phys. Rev. Letters* 11, 554 (1963); R. W. Stark and D. C. Tsui, *J. Appl. Phys.* 39, 1056 (1968).

¹¹L. Hodges, D. R. Stone, and A. V. Gold, *Phys. Rev. Letters* 19, 655 (1967).

¹²J. C. Slater, *J. Appl. Phys.* 39, 761 (1968).

¹³J. W. D. Connolly, *Phys. Rev.* 159, 415 (1967); S. Wakoh and J. Yamashita, *J. Phys. Soc. Japan* 19, 1342 (1964).

¹⁴G. S. Krinchik, *Optical Properties and Electronic Structure of Metals and Alloys*, Amsterdam, 1966, p. 484.

¹⁵S. Roberts, *Phys. Rev.* 114, 104 (1959); H. Ehrenreich, H. R. Philipp, and D. J. Olechna, *Phys. Rev.* 131, 2469 (1963).

¹⁶L. Hodges, H. Ehrenreich, and N. D. Lang, *Phys. Rev.* 152, 505 (1966).

¹⁷S. Doniach, *J. Appl. Phys.* 39, 751 (1968).

¹⁸W. H. Keesom and C. W. Clark, *Physica* 2, 513 (1935).

¹⁹E. I. Kondorskiĭ, *Zh. Eksp. Teor. Fiz.* 55, 2367 (1968) [*Sov. Phys.-JETP* 28, 1256 (1969)].